Advances in Science and Technology Research Journal

Advances in Science and Technology Research Journal, 2026, 20(9), 149–162
https://doi.org/10.12913/22998624/222559
ISSN 2299-8624, License CC-BY 4.0

Received: 2026.04.29
Accepted: 2026.07.10
Published: 2026.08.01

Experimental-numerical analysis of thin-walled box structures with integral corrugated stiffeners, subjected to torsion

Tomasz Kopecki[1*], Przemysław Alfred Mazurek[1], Aleksandra Tęczar[2], Łukasz Piotr Święch[1]

[1] Department or Mechanical Engineering and Aviation, Rzeszów University of Technology, Al. Powstańców Warszawy 8, Rzeszów, Poland
[2] Safran Aircraft Engines Poland, Research and Development Department, ul. Południowa 23, 39-120 Sędziszów Małopolski, Poland
* Corresponding author's e-mail: tkopecki@prz.edu.pl

ABSTRACT

The study presents the results of model experimental investigations and nonlinear numerical analyses of thin-walled, two-segment box structures with various configurations of integral corrugated stiffeners. The models for experimental testing were fabricated using additive manufacturing techniques. Five variants of the structure were examined, including a reference configuration without reinforcement. The experimental investigation was carried out using a dedicated test rig. Numerical representations of the investigated models were developed and subjected to nonlinear analyses using finite element method-based software. The adequacy of the numerical results was assessed through comparison with experimental data. The objective of the study was to determine the effect of different forms of the proposed structural solution on the magnitude of the critical load and the nature of post-buckling deformation.

Keywords: thin-walled structures, 3D printing, torsion, experiment, finite elements method, stiffeners.

INTRODUCTION

Contemporary aerospace engineering, despite the use of advanced materials engineering solutions and increasingly sophisticated manufacturing techniques, remains to a large extent based on conventional structural design schemes. This is particularly evident in the design of airframe load-bearing components, whose geometric configurations often arise from inherent mechanical constraints [1]. It should also be emphasized that thin-walled structures with corrugated reinforcements are used not only in aviation but also in other fields of engineering, for example in construction [2–4].

One of the structural elements commonly employed in aircraft wing structures is the spar web, which serves not only as a support for the spar caps but also as a constituent wall of a thin-walled torsion box, responsible for transferring significant torsional loads acting on the wing [5]. Although torsion box configurations may vary considerably, spar webs in most cases retain flat surfaces (Figure 1).

The engineering challenge associated with the use of conventional structural solutions lies in the fact that, under torsional loading, flat surfaces are highly susceptible to buckling induced by shear, accompanied by the development of a tension field. Since the torsion box, as a load-bearing component responsible for providing the wing with torsional stiffness, should not exhibit any form of buckling according to applicable airworthiness regulations, this necessitates the use of additional structural reinforcement elements [6].

Among the available solutions to this problem, the most common approaches include increasing the web thickness, the use of sandwich structures, reinforcing frames or additional truss-like members [7–8]. In each case, however, this leads to an undesirable increase in wing mass. Under these circumstances, it appears justified to seek alternative structural solutions that enable an increase in the critical load of the spar web, while simultaneously maintaining the structural mass or minimizing its growth.

One possible way to achieve the aforementioned objectives is the use of integral stiffening elements. These may take a wide variety of forms [9]. Among the most commonly applied solutions is isogrid-type stiffening (Figure 2) [10–11].

Such a solution has been used in aerospace structures for several decades and is characterized by high effectiveness; however, it also exhibits a number of drawbacks. First, the typically densely arranged stiffeners result in a noticeable increase in structural mass. Moreover, considering the properties of materials used in aerospace applications, its manufacturing can be problematic. In the case of metals, machining is required, leading to high material consumption. In contrast, for composite structures, the integration of the stiffeners with the skin may pose significant challenges [12–13].

An alternative solution, also widely applied, is the use of integral corrugated stiffeners, commonly referred to as corrugations (Figure 3). The concept of employing corrugated sheet metal skins dates back to the pioneering era of aerospace engineering, when designers did not yet possess sufficient understanding of buckling phenomena. Structures incorporating this solution were implemented, for example, by Junkers and Ford. In later periods, corrugated skins were used in regions of structures where buckling of the skin is not permitted [14–15].

This type of integral stiffening is characteristic primarily of metallic structures, due to the possibility of manufacturing it by means of relatively inexpensive plastic forming processes. However, in the current era of rapid development of alternative manufacturing techniques, the applicability of this type of solution should also be evaluated in the context of its use in other types of structures beyond those produced using conventional technologies.

As a result of the rapid development of electronics and significant advances in materials engineering, additive manufacturing techniques are attracting increasing interest among aircraft designers. Three-dimensional printing is currently used to produce components from both polymer-based materials and metals [16]. From the perspective of aerospace applications, multimaterial systems, representing a class of composites whose mechanical properties enable their use as one of the primary constituents of airframe structures, appear particularly promising. The continuous growth of knowledge in the development of new materials for additive manufacturing suggests that, in the near future, this technology may become as widespread as the currently

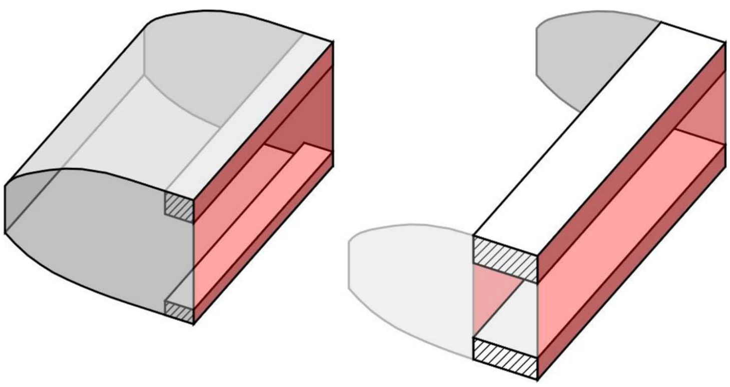

Figure 1. Examples of wing torsion boxes

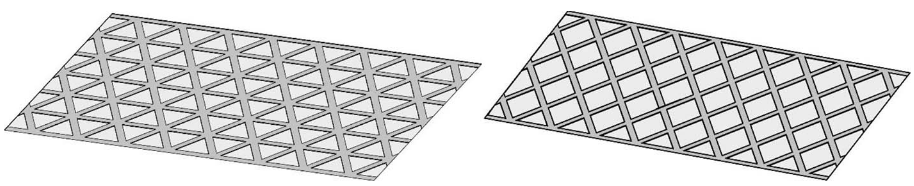

Figure 2. Examples of isogrid-type stiffening

Figure 3. Corrugated stiffening of control surfaces

employed forming methods for fiber-reinforced composites [17].

This allows solutions such as integral corrugated stiffeners to be reconsidered from a new perspective. Additive manufacturing enables virtually unrestricted freedom in shaping structural components. The formation of corrugated stiffening is likewise no longer subject to the limitations associated with conventional forming processes. It therefore appears justified to pursue research into new types of similar structural solutions.

Aircraft load-bearing structures in which integral corrugated stiffening may find application include shells of low or zero curvature that are particularly susceptible to instability, such as the aforementioned torsion box webs operating under significant torsional loading [18]. This study presents the results of experimental investigations and nonlinear numerical analyses of several variants of cross-corrugated stiffening applied to a two-section structure representing a segment of a box spar.

PURPOSE AND SCOPE OF THE STUDY

The objects of the study were thin-walled, two-segment box structures with identical principal geometric parameters, subjected to restrained torsion (Figure 4a). Both the side walls and the frames were assigned thicknesses sufficient to prevent buckling; these elements corresponded, respectively, to the wing spar caps and portions of the wing ribs, i.e. transverse structural elements. The primary components under investigation were the front and rear closing webs, of relatively small thickness, which were susceptible to buckling (Figure 4b).

In view of this characteristic, a solution in the form of selected variants of integral corrugated stiffening with a cross-oriented layout was proposed, with orientation directions corresponding to the directions of the tension field (Figure 5).

A total of five model variants, featuring different stiffening configurations, were analyzed.

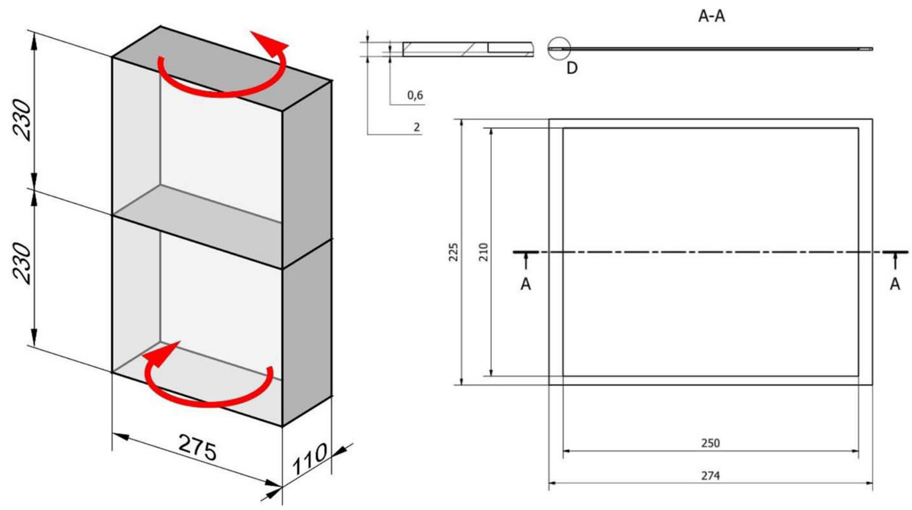

Figure 4. (a) Loading scheme and principal geometric parameters of the experimental models; (b) dimensions of the walls susceptible to buckling

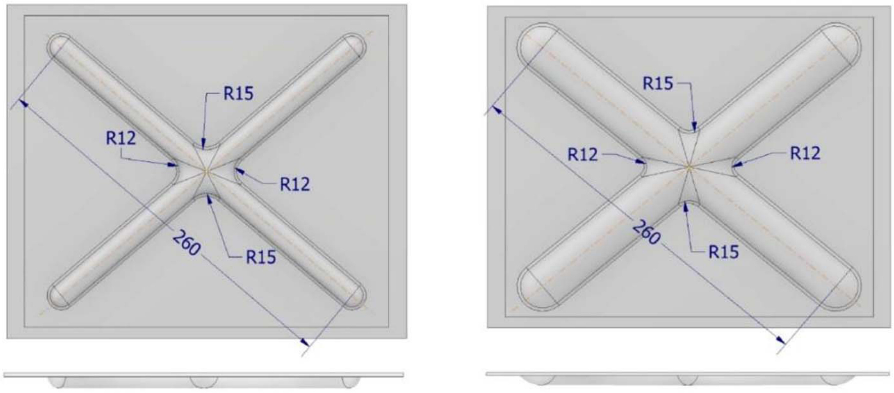

Figure 5. Investigated forms of corrugated stiffening

Variant I constituted the reference solution, without stiffeners. In Variant II, open-section corrugated stiffeners with a larger curvature of the cross-section were applied (Figure 6a). Variant IV additionally included flat closing walls (Figure 6b). In Variants III and V, corrugated stiffeners with a smaller cross-sectional curvature were used, analogously to the previous variants (Figures 6c, 6d).

It should be noted that, in Variants II and III, the corrugated stiffeners occupy a significantly smaller portion of the web surface; however, the large curvature of their cross-sections reduces their susceptibility to buckling. In the case of Variants IV and V, this susceptibility is greater; however, they also cover a larger proportion of the web surface, which contributes to an increase in the critical load of the areas between the corrugated stiffeners.

The objective of the analyses was to determine the influence of the corrugation cross-section type on the character and magnitude of web deformation, as well as on the level of the critical load. The scope of the study included advanced post-buckling deformation states. All model variants with stiffened webs were evaluated with reference to the baseline case without stiffening. The advantages and disadvantages of the individual solutions were assessed in the context of the instability effects associated with their application. Nonlinear numerical analyses were also performed, with the aim of achieving agreement between deformation patterns obtained numerically and experimentally. In the case of such agreement, the numerical model may be used to determine stress distributions that can be considered reliable based on the principle of uniqueness of solutions, according to which a given deformation state corresponds to one and only one stress distribution.

EXPERIMENTAL RESEARCH

The experiments were carried out using a test rig that enabled the application of torsional loading (Figure 7). The load was applied in a gravity-driven manner. The models were attached to the test stand using bolted connections. As the primary

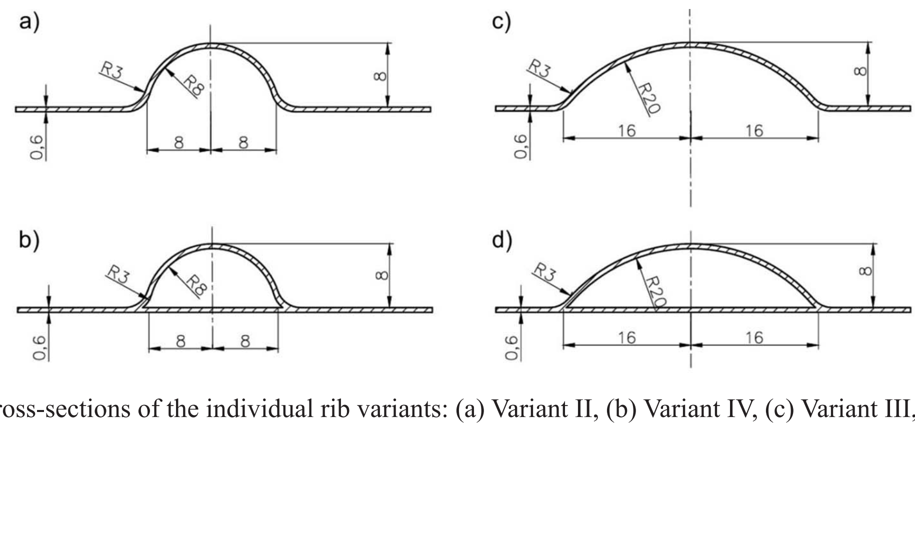

Figure 6. Cross-sections of the individual rib variants: (a) Variant II, (b) Variant IV, (c) Variant III, (d) Variant V

characteristic describing changes in the structural response, a representative equilibrium path was adopted, defined as the relationship between the total angle of twist and the applied torque. The angle of twist was measured using a micrometer sensor. The displacement of a selected point on the lever transmitting the torsional load allowed for the determination of its rotation angle, which was equal to the total twist angle of the structure. During the experiment, measurements were also performed using optical scanning systems based on digital image correlation (GOM ARAMIS) and projection moiré techniques (GOM ATOS).

All models used in the experimental investigations were fabricated using 3D printing. A commonly used biodegradable polymer, polylactic acid (PLA), characterized by linear elasticity over a relatively wide range of loads, was selected as the material. This made it possible to consider exclusively geometric nonlinearities, without the need to account for material nonlinearities.

The models for experimental investigations were manufactured using ULTIMAKER S5 devices. In order to achieve satisfactory print quality and minimize the required number of support structures, a modular design approach was adopted. Each model consisted of 12 components printed separately and subsequently assembled using adhesive bonding (Figure 8). In the case of stiffened walls, printing with support structures was necessary. To enable the formation of internal cavities in closed-section corrugated stiffeners, a polyvinyl alcohol (PVA)-based filament, characterized by water solubility, was used for the support structures. The cavities were therefore obtained through a repeated dissolution process.

The masses of the individual walls for the respective model versions are summarized in the table (Table 1).

It should be noted that the mass changes resulting from the use of stiffeners are relatively very small, considering their contribution to the total masses of the complete structures.

Due to the method of attaching the models to the test rig components, it was necessary to prefix the mounting bolts in the holes of the outer frames (Figure 9).

During the experiment, load increments of 20 N were applied. At each step, the total angle of twist of the structure was measured. This made it possible to determine the relationship between the total twist angle and the applied torque, constituting a representative equilibrium path of the system (Figure 10).

The exact values of the total twist angles for all model versions across the full load range are presented in the table (Table 2).

Measurements of displacements in selected regions of the model were also performed for successive load levels using the ARAMIS scanner, as well as displacement measurements at maximum load using the ATOS scanner.

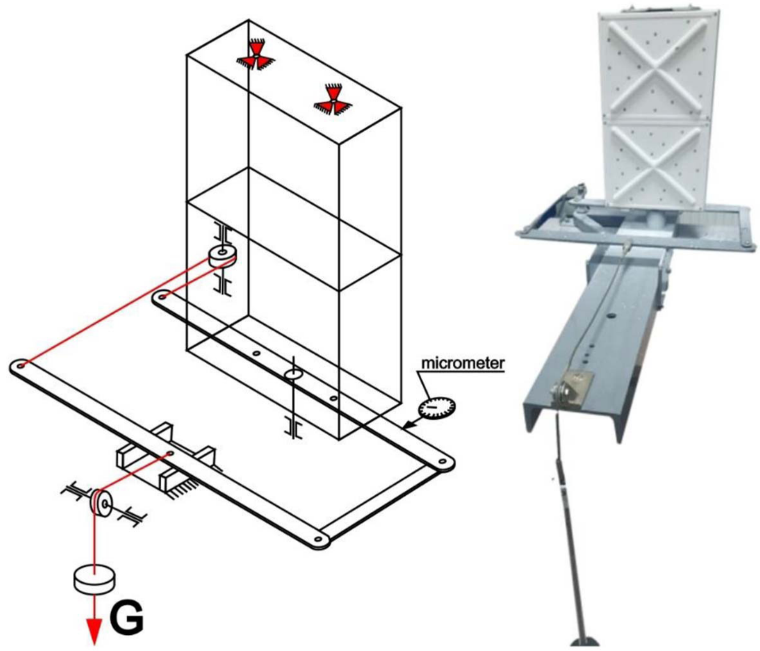

Figure 7. Experimental test rig: (a) kinematic scheme, (b) view of the test setup with the mounted model

Table 1. Summary of individual wall masses

Model version	Model mass [g]
I	60
II	67
III	63
IV	74
V	76

Although corrugations are commonly regarded as a form of integral stiffening, the experimental results indicate that, in the case of ribs with open cross-sections in the considered configuration, the structure exhibits significantly lower torsional stiffness than in the reference variant. As expected, the tension fields induced by the applied loading led to the occurrence of post-buckling

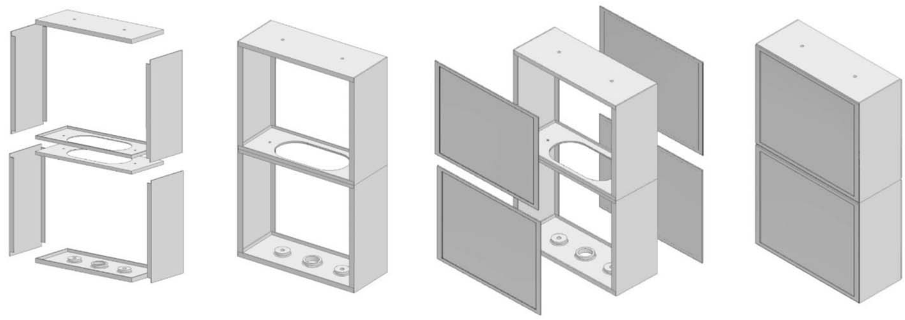

Figure 8. Assembly stages of the models for experimental testing

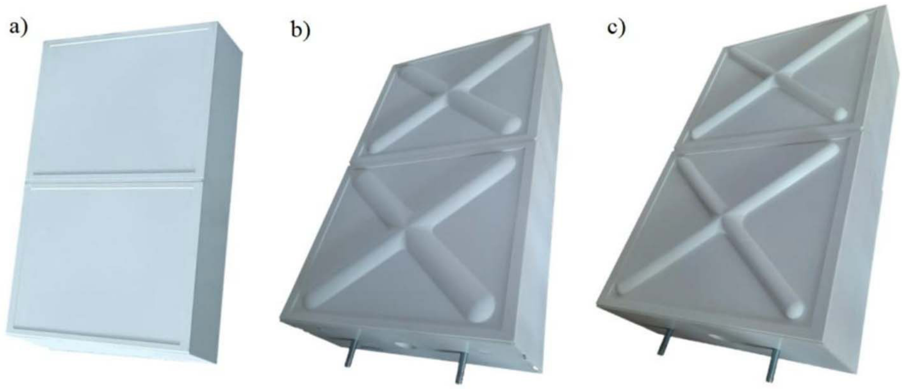

Figure 9. Views of the experimental models: (a) Variant I, (b) Variants IV–V, (c) Variants II–III

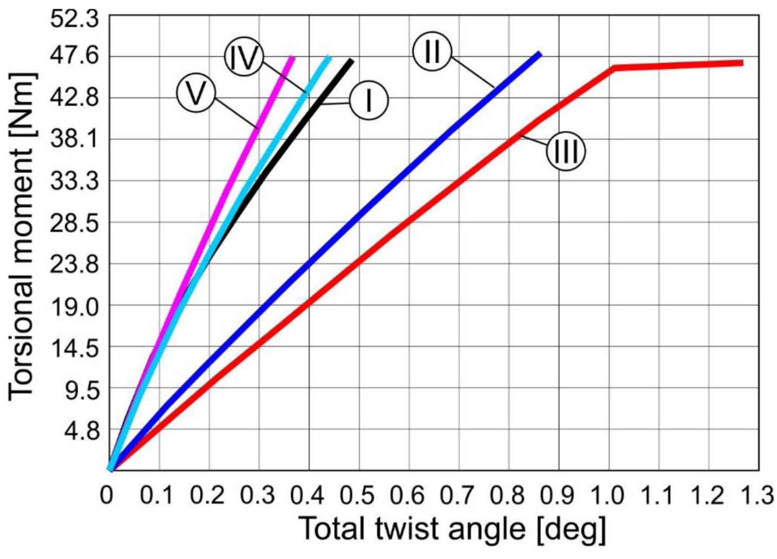

Figure 10. Comparison of representative equilibrium paths for the individual variants of the investigated structures

Table 2. Total twist angles [deg]. M_T – torsional moment [NM]

M_T	Version I	Version II	Version III	Version IV	Version V
4.8	0.032	0.074	0.085	0.027	0.031
9.5	0.067	0.154	0.167	0.06	0.066
14.3	0.11	0.235	0.248	0.098	0.102
19	0.145	0.322	0.334	0.139	0.138
23.8	0.193	0.409	0.424	0.18	0.176
28.5	0.246	0.491	0.519	0.23	0.213
33.3	0.295	0.585	0.611	0.276	0.252
38.1	0.349	0.684	0.716	0.331	0.294
42.8	0.405	0.772	0.819	0.385	0.334
43.66	-	-	0.838	-	-
44.85	-	-	0.966	-	-
47.6	0.458	0.867	-	0.436	0.374

deformations in the form of characteristic triple-wave patterns (Figure 11a). The first visible signs of instability in the observed front webs appeared at approximately 10% of the maximum load.

The occurrence of advanced post-buckling deformations in aerospace structures is generally considered acceptable for most regions of semi-monocoque skins. However, this phenomenon should not occur in wing torsion box components, which are responsible for maintaining torsional stiffness. This limitation therefore rules out the solution applied in the reference model, creating the need for effective stiffening that does not result in a significant increase in structural mass.

The reduction in structural stiffness observed in Variants II and III was caused by deformations of the corrugations themselves, particularly those oriented transversely to the direction of tension within the tension field. This leads to a bending effect, resulting in a significant increase in web deformation (Figure 12). Moreover, as deformation increases, the curvature of the corrugated stiffener cross-section decreases, which makes the stiffener more susceptible to buckling. In Variant III, this led to buckling of the shell segment forming the corrugated stiffener in the intersection region (Figure 11c). This effect was reflected in the representative equilibrium path (Figure 10) as a distinct kink in the curve, indicating a sudden increase in the twist angle. These results suggest that, for open-section corrugated stiffeners, increasing their width while reducing their cross-sectional curvature not only decreases the structural stiffness but also increases the risk of global buckling.

In both variants with open-sections corrugated stiffeners, the effect of early instability associated with the formation of deep folds was eliminated. In the case of Variant II, no effects equivalent to structural failure were observed (Figure 11b). From the standpoint of deformation distribution,

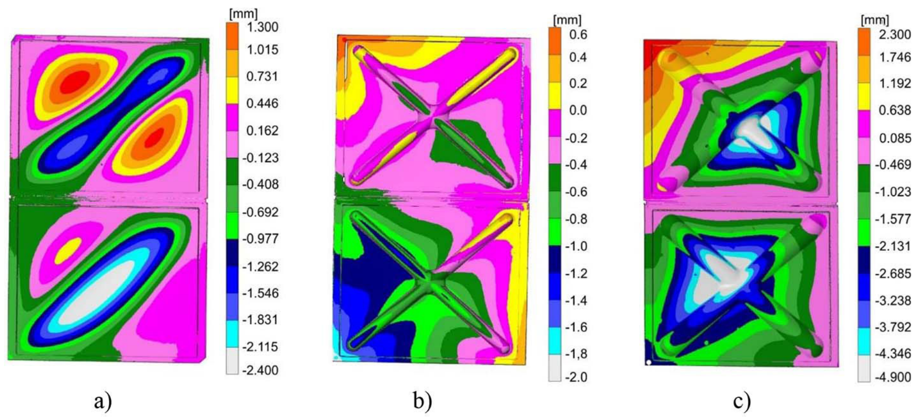

Figure 11. Distributions of transverse displacements determined using the ATOS scanner at maximum load: (a) Variant I, (b) Variant II, (c) Variant III

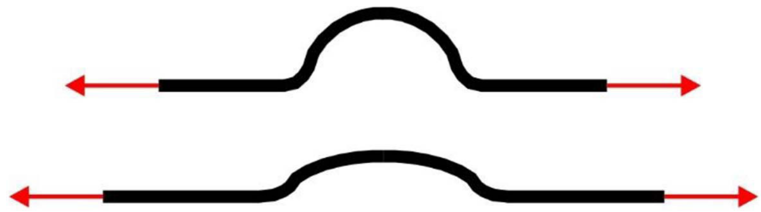

Figure 12. Stages of transverse deformation of the corrugation cross-section in the direction of tension

this solution appears advantageous; however, as noted, it is accompanied by a significant increase in the total twist angle of the structure compared to the reference variant.

The application of closed-section corrugated stiffeners in Variants IV and V resulted in a clear increase in the torsional stiffness of the structure. This can be attributed to the closing walls at the stiffener bases, which effectively prevented the previously described deformation of the stiffener cross-sections. In these variants, the stiffeners form closed cross-sectional perimeters characterized by high torsional rigidity. This stiffness is proportional to the Bredt area, which explains the higher torsional stiffness of Variant V compared to Variant IV. Moreover, scan results at maximum load revealed the occurrence of undesirable deformation modes in the latter case (Figure 13a).

Although the integral stiffening prevented the formation of folds characteristic of the tension field, local instability effects occurred in the regions between the stiffeners. These were not clearly reflected in the representative equilibrium path; however, their presence should be regarded as a disadvantage of this solution variant. Increasing the base width of the corrugated stiffeners reduces the area of flat regions between them, thereby limiting their susceptibility to buckling. This is confirmed by the displacement distribution for Variant V (Figure 13b). In this case, the web deformations exhibit a continuous character, without localized instability zones. Therefore, the variant with widened closed-section corrugated stiffeners can be regarded as the most advantageous among the investigated solutions. It should be noted, however, that the shell segments forming the closing walls of the closed-section stiffeners are also susceptible to buckling, and this susceptibility increases with their surface area. Therefore, further increasing the width of the corrugated stiffeners may lead to the occurrence of undesirable deformation modes. Moreover, increasing the corrugation width reduces the curvature of its cross-sectional contour, which in turn increases the susceptibility of the stiffener to global buckling, as observed in Variant III.

NUMERICAL ANALYSES

The numerical calculations were based on the finite element method. In order to capture

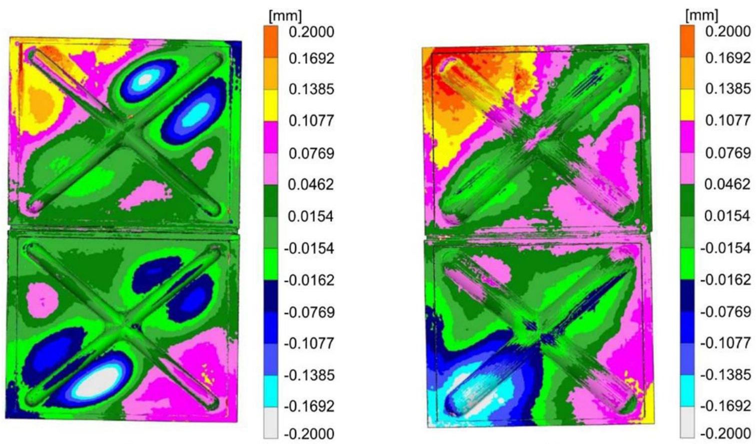

a) b)

Figure 13. Distributions of transverse displacements determined using the ATOS scanner at maximum load: a) Variant IV, b) Variant V

complex deformation patterns, including post-buckling behavior, it was necessary to perform nonlinear analyses. Due to the elastic nature of the deformations, only geometric nonlinearities were considered in the calculations, while a linear material model was retained. The numerical analyses were carried out using Ansys Workbench 2024 R2.

Although the material produced by additive manufacturing exhibits slight orthotropy, previous experiments indicate that the orthotropy effect decreases as the number of layers used during the printing process increases. The material itself, as a polymer, is characterized by isotropic mechanical properties. Any potential orthotropy depends both on the print quality, namely the cohesion between deposited layers/paths, and on the printing pattern or strategy. In the case of higher-end printers, the issue of orthotropy becomes negligibly small. Therefore, it was assumed that a simplified isotropic material model could be applied in the calculations. The material properties of PLA were taken from previously conducted experiments [19], with the following values: E=3300 MPa, ν=0.34.

The essence of nonlinear analysis lies in determining the equilibrium path, defined as the relationship between the structural state—described by values corresponding to individual degrees of freedom—and a control parameter associated with the applied load. In discrete systems, which constitute simplified models of continuous systems, the equilibrium path is a hypersurface in the state hyperspace [20-21], the dimensionality of which corresponds to the number of degrees of freedom of the system. The analysis is performed incrementally, through successive load steps corresponding to load increments. At each of these steps, the discrete system satisfies the residual force equilibrium equation [22]:

$$\boldsymbol{r}(\boldsymbol{u},\lambda)=\boldsymbol{0} \quad (1)$$

In this equation, $\boldsymbol{u}$ is the state vector, whose components correspond to the nodal displacements of the structure in its current geometric configuration at a given incremental step, while $\boldsymbol{\lambda}$ is the control parameter, proportional to the magnitude of the applied load. The residual vector $\boldsymbol{r}$ contains the unbalanced force components corresponding to the current deformation state. The incremental phase consists in transitioning from state n to state $n+1$, to which the following increments correspond:

$$\Delta\boldsymbol{u}_n=\boldsymbol{u}_{n+1}-\boldsymbol{u}_n,\ \Delta\lambda_n=\lambda_{n+1}-\lambda_n \quad (2)$$

In currently used software, incremental procedures are supplemented with a correction phase that enables the determination of the above quantities. This is an iterative procedure aimed at satisfying the so-called incremental constraint equation, also referred to as the constraint equation [22]:

$$c(\Delta\boldsymbol{u}_n,\Delta\lambda_n)=0 \quad (3)$$

The correction strategy, which determines the specific form of the equation, is defined by the user. The geometric characteristics of the investigated structures did not necessitate the use of a correction strategy based on arc-length control (Riks method) or hyperspherical correction (Crisfield method). In the case of Variant III, a snap-through response associated with global buckling of the shell in the region of the corrugation root subjected to compression was anticipated; however, this effect was preceded by a series of post-buckling deformations, and thus the instability did not occur as a sudden process that could lead to singularities in the representative equilibrium path. Consequently, for all nonlinear analyses, the Newton–Raphson prediction method with load control correction was employed [23].

The geometric models were created using SpaceClaim 2024 R2, dedicated to the employed software. Finite element meshes for all model variants were developed based on a series of preliminary linear analyses, using an appropriate control tool provided by the software (Figure 14a). The numerical model was based on the use of two-dimensional shell elements with linear shape functions. Depending on the variant, the models comprised from 6.996 elements (Variant I) to 20,824 elements (Variant IV).

The boundary conditions and load application were modeled with high fidelity to the experimental setup (Figure 14b).

Below, distributions of displacements for the analyzed structures are presented (Figures 15–19), together with corresponding images obtained experimentally using optical scanners. In all cases, the results refer to the stage of maximum load application. Comparisons of representative equilibrium paths obtained from both experimental and numerical analyses are also provided (Figures 20–24).

Both the displacement distribution comparisons and the representative equilibrium paths demonstrate satisfactory agreement between the

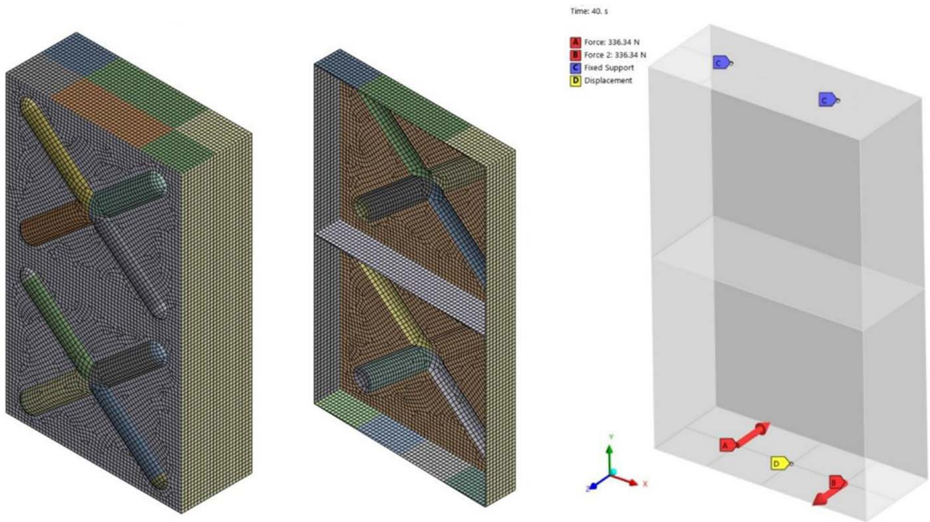

a) b)

Figure 14. (a) Example of the finite element mesh for Variant III, (b) model of boundary conditions and load application

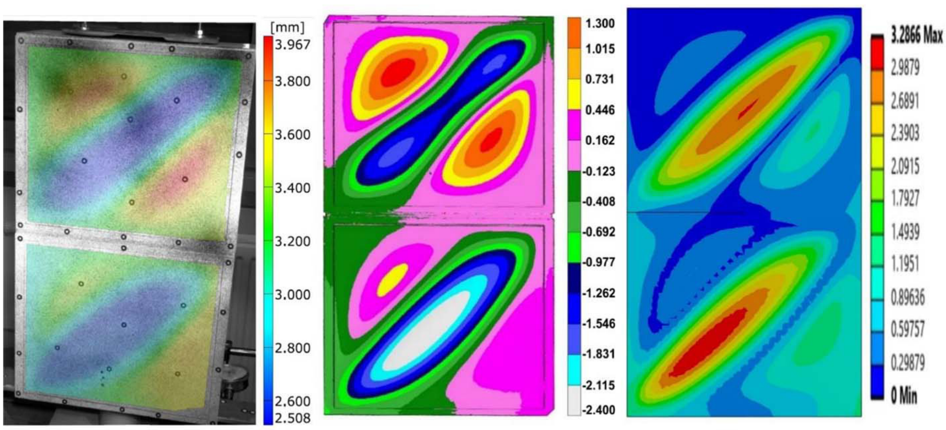

a) b) c)

Figure 15. Distributions of transverse displacements for Variant I of the structure: (a) ARAMIS scanner, (b) ATOS scanner, (c) numerical analysis

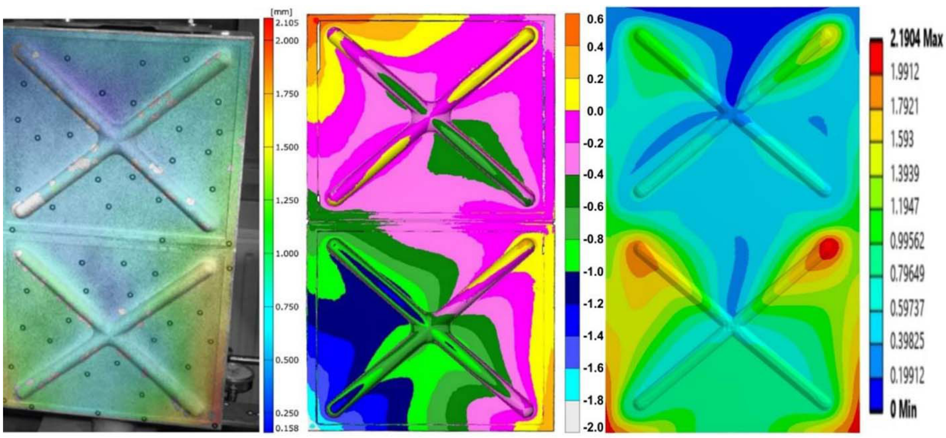

a) b) c)

Figure 16. Distributions of transverse displacements for Variant II of the structure: (a) ARAMIS scanner, (b) ATOS scanner, (c) numerical analysis

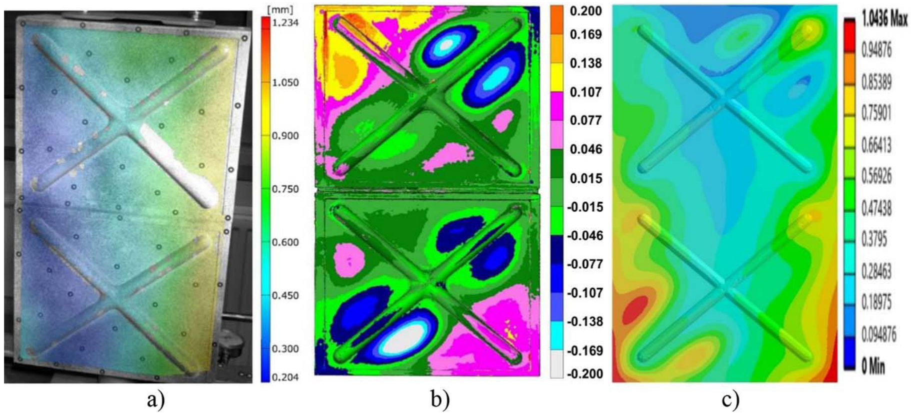

Figure 17. Distributions of transverse displacements for Variant IV of the structure: (a) ARAMIS scanner, (b) ATOS scanner, (c) numerical analysis

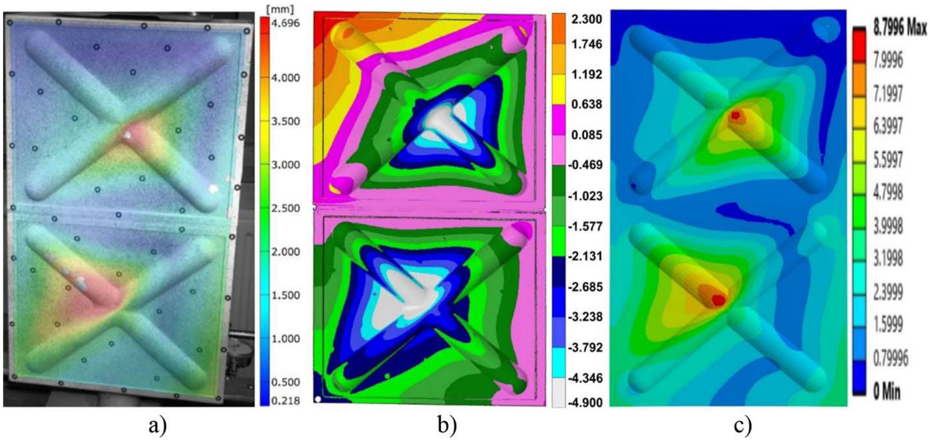

Figure 18. Distributions of transverse displacements for Variant III of the structure: (a) ARAMIS scanner, (b) ATOS scanner, (c) numerical analysis

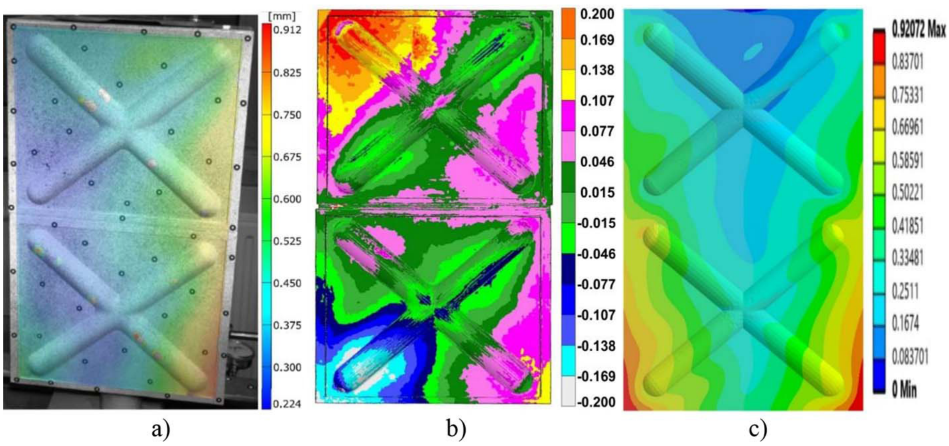

Figure 19. Distributions of transverse displacements for Variant V of the structure: (a) ARAMIS scanner, (b) ATOS scanner, (c) numerical analysis

experimental results and the nonlinear numerical analyses. This confirms the high quality of the numerical models and the appropriate selection of procedures used in the analyses. The largest error was recorded for Variant III of the structure; however, considering the nature of the physical phenomenon reproduced numerically, the analysis result should be regarded as satisfactory. The

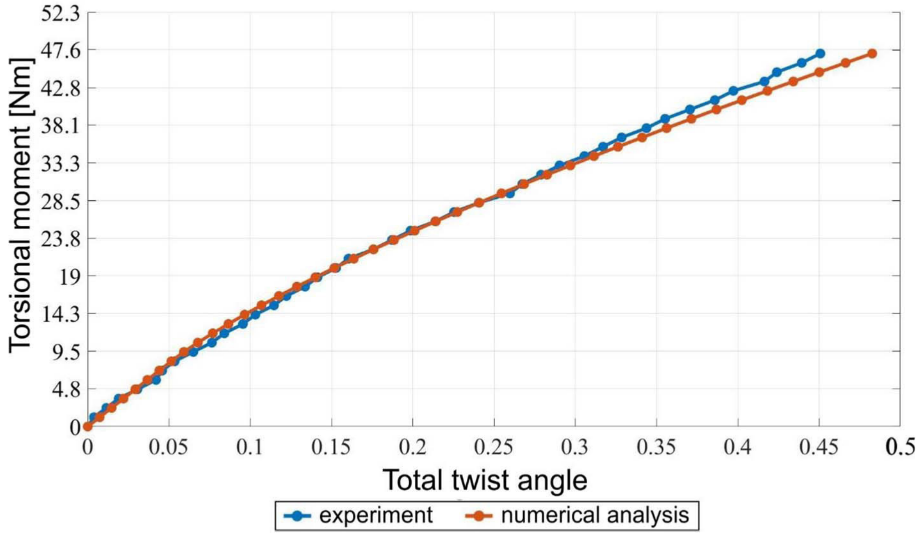

Figure 20. Comparison of representative equilibrium paths for Variant I of the structure

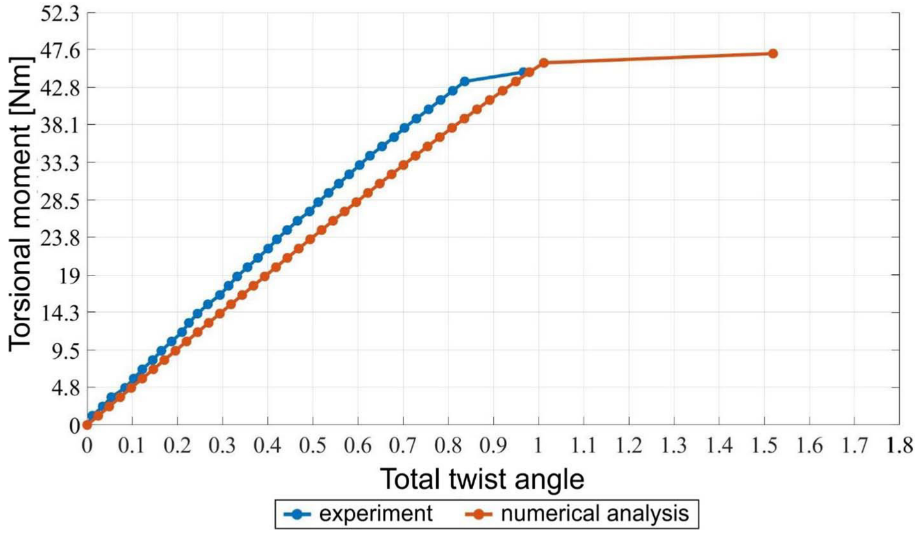

Figure 21. Comparison of representative equilibrium paths for Variant III of the structure

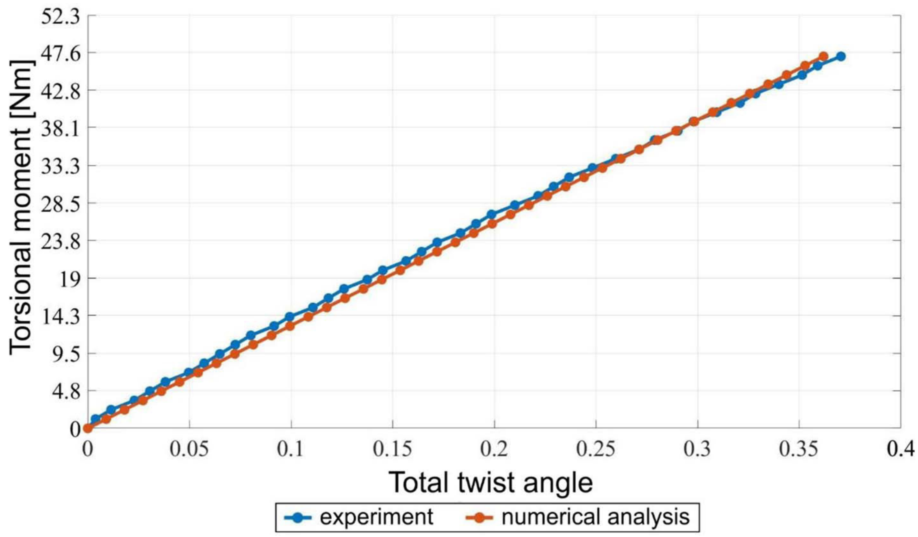

Figure 22. Comparison of representative equilibrium paths for Variant V of the structure

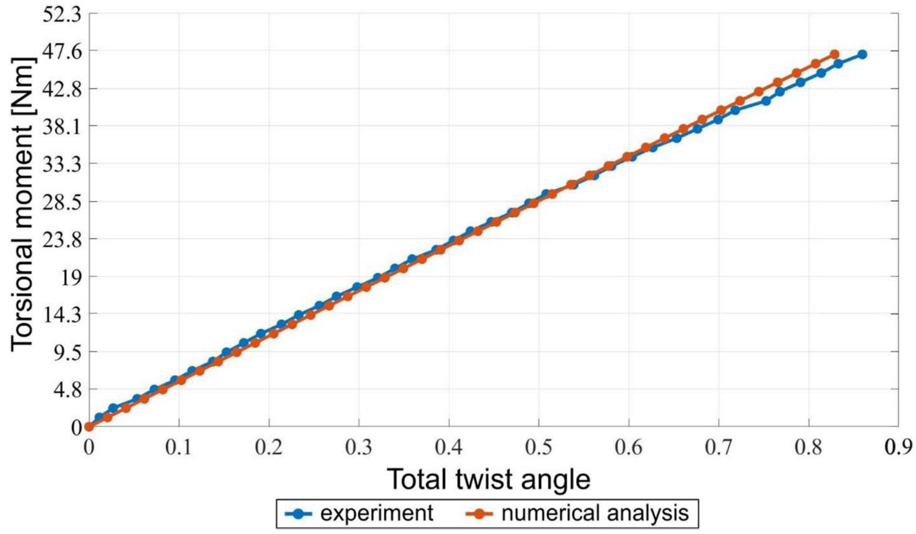

Figure 23. Comparison of representative equilibrium paths for Variant II of the structure

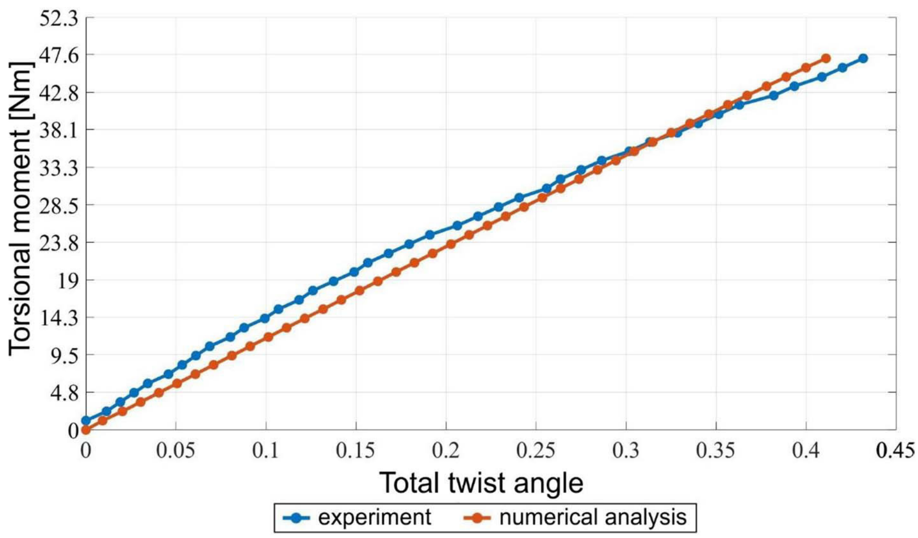

Figure 24. Comparison of representative equilibrium paths for Variant IV of the structure

most critical aspect in this case is the load value at which global buckling of the corrugation occurred. The error of the numerical solution relative to the experimental result does not exceed 1%, and can therefore be considered negligible.

CONCLUSIONS

The results of the experimental investigations and nonlinear numerical analyses confirmed the applicability of the proposed solution, while also revealing a number of key factors influencing its performance. In particular, it should be noted that the use of corrugations with open cross-sections significantly reduces the structural stiffness. At the same time, the critical load increases; however, in the case of load-bearing components such as spar webs, which also form part of the torsion box, ensuring sufficient stiffness is essential.

Therefore, the use of corrugated stiffening with closed cross-sections appears to be a more appropriate solution, as it contributes both to an increase in the critical load and to the overall stiffness of the structure. Although such a solution is difficult to implement using conventional manufacturing techniques, it can be realized relatively easily using additive manufacturing.

It can therefore be inferred that it would be beneficial to develop a procedure enabling the optimal selection of geometric parameters of the stiffening, based on a chosen criterion for example, the maximum load at which any form of instability occurs within the structure. This would require conducting an extensive range of numerical analyses, potentially supported by the use of artificial neural networks.

In light of the achieved agreement between the numerical analyses and the experimental results, it can be concluded that the proposed numerical model is valid and may be used to determine stress components within the validated range of loading and deformation. The applied numerical procedures do not require modification. It is also not necessary to introduce any form of initial geometric imperfections into the model.

From the perspective of further research, it appears advisable to modify the stiffening system by increasing the number of stiffeners while simultaneously reducing the cross-sectional area of each individual element.

REFERENCES

1. Dobrzański P, Czarnocki P, Lorenz Z, Shell structures – theory and application, CRC Press. 2013.
2. Chang G.Y, ShiJinyong X., Experimental and numerical study of cold-formed steel shear walls with corrugated steel plate, Thin-Walled StructuresJune 2026; 225: 114783.
3. Kalantari O., Asl H. E., Performance evaluation of a novel compound steel shear wall section combining flat and corrugated plates, Structures 2026; 87: 11691.
4. Ye Y., Jiansong X., Xiuxian J., Guofu D., High-performance bending in 3D-printed reinforced-rib corrugated composites via continuous fiber additive manufacturing: A hybridexperimental-computational approach, Thin-Walled Structures 2025; 217: 113905.
5. Kopecki T, Bakunowicz J, Lis T, Post-critical deformation states of composite thin-walled aircraft load-bearing structures, Journal of Theoretical and Applied Mechacnics; 2016; 54(1): 195–204.
6. Arborcz J, Post-buckling behavior of structures, Numerical techniques for more complicated structures, Lecture Notes In Physics 1985; 288: 83–142.
7. Kopecki T, Numerical-experimental analysis of the post-buckling state of a multi-segment multi-member thin-walled structure subjected to torsion, Journal of theoretical and applied mechanics; 2011; 49(1): 227–242.
8. Singh K., Kapania R.K, Optimal Design of Tow-Steered Composite Laminates with Curvilinear Stiffeners, 2018 AIAA/ASCE/AHS/ASC Structures, Structural Dynamics, and Materials Conference, 8–12 January 2018.
9. Święch, Ł. Experimental and numerical studies of low-profile, triangular grid-stiffened plates subjected to shear load in the post-critical states of deformation. Materials 2019; 12: 3699.
10. Wang D., Abdalla M., Zhang W., Buckling optimization design of curved stiffeners for grid-stiffened composite structures, Composite Structures 2016.
11. Lynch C. A., Finite element study of the post buckling behavior of a typical aircraft fuselage panel, PhD Thesis, Queen's University Belfast 2000.
12. Huybrechts S, Tsai SW, Analysis and behavior of grid structures, Composites science and technology; 1996; 56: 1001–1015.
13. Wang D., Abdalla M., Zhang W., Buckling optimization design of curved stiffeners for grid-stiffened composite structures, Composite Structures 2016.
14. Tewari K., Pandit M.K., Budarapu P.R., Natarajan S., Analysis of sandwich structures with corrugated and spiderweb-inspired cores for aerospace applications, Thin-Walled Structures 2022; 180: 109812.
15. Chen-Bao W., Bo-Li Z., Hao-Jun S., Yan-Lin G.,*, Wen-Jin Z., Li-Lan D., Global stability design of double corrugated steel plate shear walls under combined shear and compression loads, Thin–Walled Structures 2024; 199: 111789.
16. Monaldo E., Ricci M., Marfia S. Mechanical properties of 3D printed polylactic acid elements: Experimental and numerical insights, Mechanics of Materials 2023; 177: 104551.
17. Kratochvíl J., Sadilek M., Musil V., Stančeková D., The effectiveness of strategies printing printer easy 3D maker, Advances in Science and Technology Research Journal 2018; 12(2): 197–205.
18. Kopecki H., Kopecki T., Święch Ł., Issues of aircraft structural strength, Rzeszów University of Technology Publishing House, Rzeszów, 2023.
19. Kopecki T., Święch Ł., Experimental-numerical analysis of a flat plate subjected to shearing and manufactured by incremental techniques, Advances in Science and Technology Research Journal 2023; 17(4): 179–188.
20. Felippa CA, Crivelli LA, Haugen B, A survey of the core-congruential formulation for nonlinear finite element, Archive of Computer Methods in Engineering 1994.
21. Felippa C. A., Procedures for computer analysis of large nonlinear structural system in large engineering systems, ed. by A. Wexler, Pergamon Press, London, UK 1976.
22. Crisfield MA, Non-linear finite element analysis of solid and structures, J. Wiley & Sons. 1997.
23. Doyle JF, Nonlinear analysis of thin-walled structures, Springer-Verlag. 2001.